

# Molecular Dynamics Benchmarks for Size-Dependent Tension, Bending, Buckling, and Vibration of Nanobeams\*

Hossein Darban<sup>1</sup>

*Institute of Fundamental Technological Research, Polish Academy of Sciences, Pawińskiego 5B, 02-106 Warsaw, Poland*

## Abstract

Nonclassical continuum mechanics-based modeling of small-scale structures, such as micro- or nanobeams, is a prominent research topic that has been extensively investigated and is also beneficial for designing small-scale intelligent devices. The accuracy of size-dependent beam models remains untested in many instances within the literature due to the scarcity of experimental and molecular dynamics (MD) results at small scales. This paper aims to provide comprehensive MD benchmark solutions that facilitate verifying nonclassical continuum models for miniaturized beams under tension, bending, buckling, and free transverse vibration. Size-dependent Young's moduli, bending stiffnesses, buckling loads, and natural frequencies are presented through large-scale MD simulations involving up to one million atoms for silicon (Si) nanobeams with square or rectangular cross-sections. The size effects that arise from the scaling effect (where all dimensions of the nanobeams change proportionally) and variations in thickness and length are systematically studied. The findings demonstrate that the size effect depends on the type of mechanical problem and the aspect ratio of the nanobeams. In all cases, the silicon nanobeams demonstrate a softer mechanical response as their dimensions decrease.

**Keywords:** Size effect; Nonclassical continuum mechanics; Atomistic models; Silicon; Calibration.

## 1. Introduction

Miniaturization of electromechanical devices is a trend within the Engineering Science community that has significantly contributed to modern technology and is helping to shape a promising future. Thanks to this innovation, there are micro- and nanoelectromechanical systems (MEMS and NEMS) with critical applications in different fields that operate with minimal energy and perform multitasking with high precision [1,2]. Many of these smart systems include simple mechanical elements such as micro- or nanobeams. For instance, scientists can measure the weight of a single cell by using ultrasensitive nanomechanical mass sensors [3]. In this case, the mass sensor is often a micro- or nanocantilever.

---

<sup>1</sup>- *Corresponding author: Hossein Darban; E-mail address: [hdarban@ippt.pan.pl](mailto:hdarban@ippt.pan.pl); Tel.: (+48) 22 826 12 81*

\* This is a preprint of a manuscript currently under review at a peer-reviewed journal. This version has not undergone peer review. The preprint is released under the CC BY 4.0 license.

The trend toward miniaturizing systems accounts for the extensive study of mechanical modeling of micro- and nanostructures such as beams[4–14]. The outcome of this line of research is the development of several advanced structural theories based on nonclassical continuum mechanics models, such as couple stress theory [15], strain gradient theory [16], micropolar theory [17], nonlocal elasticity [18], surface elasticity theory [19], theories based on fractional calculus [20], modified couple stress theory [21], modified strain gradient theory [22], and nonlocal strain gradient theory [23]. A detailed discussion of some of these theories can be found in [24]. The current trend involves integrating these models to benefit from a wider range of advantages. As a recent example, the mixture unified gradient theory of elasticity integrates the stress gradient model, the strain gradient model, and classical elasticity theory [25,26]. The common feature of these structural theories is their capability to capture size effects as the dimensions of structures decrease.

Nevertheless, there is a critical issue that casts doubt on the efficacy of size-dependent structural theories, as most formulated models are neither validated against experimental results nor atomistic data obtained by, for instance, molecular dynamics (MD). Therefore, the question remains whether these nonclassical models predict accurate data that can be used confidently in the design of MEMS and NEMS. However, regarding experimental validations, this is understandable given the inherent difficulties of experimentation at small scales. Nevertheless, there are a limited number of works in the literature where experimental data has been used to validate size-dependent structural theories, for instance [22,27–33]. There are some articles in the literature in which the authors use atomistic results to calibrate their formulated size-dependent structural theory, e.g., [34]. In [35], natural frequencies of free transverse vibration of Ag, Cu, and Ni nanobeams with clamped-free and clamped-clamped boundary conditions are determined through MD simulations. The effect of variation in length, thickness, and width of the nanobeams on the frequencies is studied in some cases, and the MD results are used to verify beam formulations considering surface effects. A similar study on silicon nanobeams is presented in [36]. In [37], MD results are used to assess the accuracy of local and nonlocal Timoshenko beam formulations to determine the natural frequencies of free transverse vibration of single-walled carbon nanotubes (SWCNT). A set of MD simulations is conducted in [38] to investigate size-dependent elastic properties of silicon nanocantilevers. Calculations are based on flexural and longitudinal vibrations and tension tests. It is found that smaller silicon nanocantilevers are softer than larger ones. The frequencies of a circular nanoplate determined by MD simulations are used in [39] to study the performance of several size-dependent structural models based on nonclassical continuum mechanics. The nonlocal buckling formulations for SWCNTs are verified in [40,41] by comparing the analytical results with those predicted by MD simulations.

Although atomistic simulations such as MD modeling could have been used to verify size-dependent structural theories, surprisingly, a very low percentage of the published works include such verifications. The main reason is the lack of availability of comprehensive MD benchmark solutions for the size-dependent mechanical response of small-scale structures. This work aims to address this gap by presenting a comprehensive set of MD benchmark solutions for the size-dependent tension, bending, buckling, and free transverse vibration of nanobeams. Given the wide application of silicon in MEMS and NEMS, the MD simulations are conducted on silicon nanobeams. Three distinct types of size effects are examined: (i) the scaling effect, in which the length, in-plane thickness, and out-of-plane width of the nanobeams change proportionally; (ii) the thickness effect, where only the in-plane thickness varies while the other dimensions remain fixed; and (iii) the length effect, where the length is altered while keeping the other dimensions constant. The size effect due to changes in the out-of-plane width is not explored.

The present study has the following novelties, inter alia:

- A comprehensive set of size-dependent results is presented for four different mechanical problems: tension, bending, buckling, and free transverse vibration. This makes the paper an appropriate reference for a wide range of formulations.
- The paper presents results for nanobeams with different aspect ratios appropriate for beam formulations with consideration of shear deformations.
- The paper presents results based on large-scale MD simulations containing up to a million atoms, which allows capturing a wider spectrum of the size effect.

The rest of the paper is structured as follows. The MD simulations are described in detail in Section 2. The benchmark solutions are presented in Section 3. The results are presented separately for each of the four mechanical problems. The concluding remarks are presented in Section 4.

## **2. Molecular Dynamics Simulations**

The classical molecular dynamics (MD) is used in this work to study the size-dependent response of the nanoscale beams under tension, bending, buckling, and transverse free vibration. The MD simulations are conducted using the Large Scale Atomic/Molecular Massively Parallel Simulator (LAMMPS) [42] and the obtained results are visualized using the Visual Molecular Dynamics (VMD) software [43]. The simulations are conducted on silicon (Si) nanobeams with square or rectangular cross-sections. Due to its favorable mechanical, thermal, and electrical properties, silicon is a key material for fabricating elements in MEMS and NEMS systems. Several interatomic potentials, including the Tersoff [38], Modified Embedded Atom Method (MEAM) [44], Environment-Dependent Interatomic Potential

(EDIP) [36], and Stillinger-Weber (SW) [45] potentials are commonly used in the literature for MD modeling of the mechanical response of silicon. The SW potential is chosen in this study due to its balanced trade-off between computational efficiency and accuracy, making it well-suited for large-scale simulations.

The simulations are run in a 3D domain using non-periodic (shrink-wrapped) boundary conditions in all three directions, which is appropriate for modeling the deformation of a finite beam with a rectangular cross-section. A time step of 1 fs is considered throughout the simulations. In the simulation setup, the lattice structure of the silicon beam is defined using a diamond cubic configuration with a lattice constant of 5.43 Å, oriented such that the  $x$ -axis is aligned with the  $[00\bar{1}]$  crystallographic direction, the  $y$ -axis with  $[010]$ , and the  $z$ -axis, along the length of the beam, with  $[100]$  (see Fig. 1). After defining the initial positions of the silicon atoms, the system is first minimized utilizing the conjugate gradient method using stopping tolerance for energy and force equal to  $1 \times 10^{-8}$  and  $1 \times 10^{-10}$  eV/Å, respectively. This minimization step helps to remove any residual stresses by relaxing the atomic positions to a local minimum energy configuration. Following minimization, the system is equilibrated for 100 ps at the temperature of 1 K using the NVT ensemble, where the temperature is controlled using a Nose-Hoover thermostat. The internal forces and dimensions of the system are computed and monitored during this phase to ensure the system is properly equilibrated before mechanical testing.

## 2.1. Tension

For the tension tests, the beam is divided into three different regions, namely, lower, middle, and upper, as shown in Fig. 1. The length of the beam along the  $x$ ,  $y$ , and  $z$  axes is  $L_x$ ,  $L_y$ , and  $L_z$ . The lengths of the upper and lower regions are the same and equal to  $0.1L_z$ . The atoms inside the upper region are moved with a constant velocity corresponding to the desired strain rate along the  $z$ -axis. At the same time, their movements along the other axes are restricted. The next section will present the applied strain rates for each case. The atoms inside the lower region remain fixed. This setup simulates the uniaxial tension along the  $z$ -axis, allowing the beam to elongate under displacement-controlled conditions. During the deformation, the temperature is kept constant and equal to 1 K using the NVT ensemble.

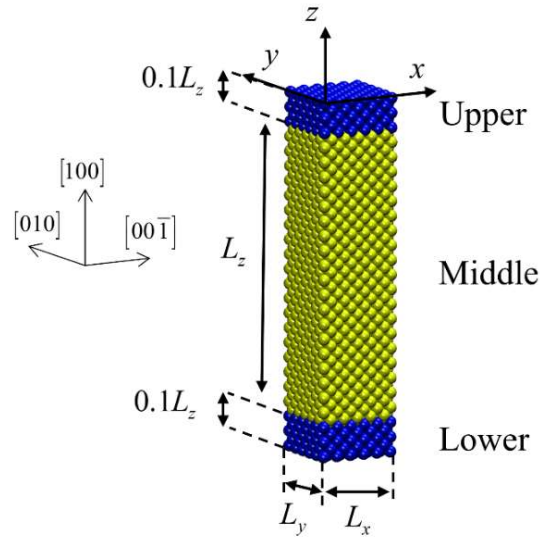


**Fig. 1** Initial configuration of the silicon nanobeam for the tensile, bending, and buckling tests.

During the simulation, strain and stress along the  $z$ -axis are calculated each time step. The strain is derived from the displacement of the upper region relative to the initial length of the beam,  $L_z$ , while the stress is computed based on the force exerted on the upper or lower regions, normalized by the initial cross-sectional area of the beam,  $L_x \times L_y$ . Temperature, potential energy, kinetic energy, and other relevant properties are averaged over time intervals and recorded to track the evolution of the system under tensile loading. For all the conducted tensile simulations, the applied strain remains around 1% to ensure a linear elastic response. The undeformed and deformed silicon nanobeams are shown in Fig. 2.

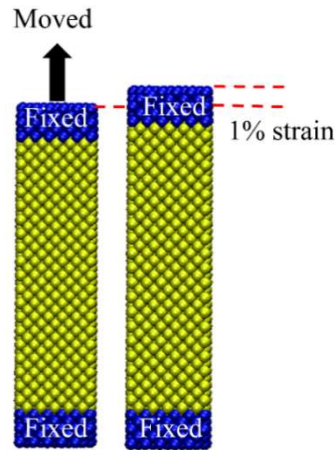


**Fig. 2** Undeformed and deformed silicon nanobeam after the tensile deformation.

The Young's modulus of silicon along the  $[100]$  crystallographic direction is determined using two methods. The first method calculates Young's modulus directly from the stress-strain curve. The second method determines the Young's modulus,  $E$ , using the following formula:

$$E = \frac{1}{V} \left( \frac{d^2U}{d\varepsilon^2} \right) \quad (1)$$

where  $V = L_x L_y L_z$  is the volume of the beam. The parameters  $U$  and  $\varepsilon$  represent the strain energy and the applied strain, respectively. The strain energy is obtained from the change in potential energy. Since the deformation remains within the linear elastic regime, a second-order polynomial curve is fitted to the strain energy-strain data points. This curve is then used to calculate the Young's modulus using Eq. (1). For all examined cases, the Young's modulus determined by both methods is within a 1% margin of difference.

## 2.2. Bending

The bending simulations are like the tension tests, with the difference being the direction of the applied displacement to the atoms in the upper region. In these simulations, the atoms in the upper region are displaced at a constant velocity corresponding to the desired deformation rate along the  $x$ -axis. At the same time, their movement in the other directions is constrained. During the deformation, the temperature is kept constant and equal to 1 K using the NVT ensemble. The deformation rate for each case will be presented in the next section. To maintain a linear elastic response, the displacement applied during the bending simulations is limited to less than 2.5% of the length of the beam. This configuration models the bending of a fixed-guided beam, as depicted in Fig. 3.

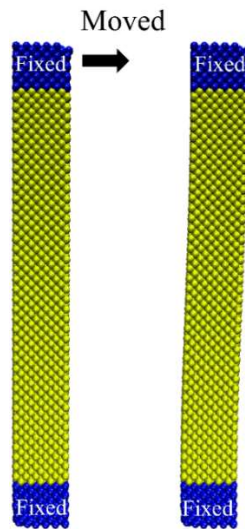


**Fig. 3** Undeformed and deformed silicon nanobeam after the bending deformation.

The primary objective of the bending simulations is to determine the bending stiffness, defined as the force along the  $x$ -axis exerted on the upper region divided by the corresponding displacement. Similar to the calculation of Young modulus, two methods are employed to determine the bending stiffness of the

silicon nanobeams. In the direct method, the bending stiffness is obtained as the slope of the load-displacement curve. In the second method, the bending stiffness,  $k$ , is calculated using the following formula:

$$k = \frac{d^2U}{d\delta^2} \quad (2)$$

where  $U$  and  $\delta$  represent the strain energy and the applied displacement, respectively. Similar to the tension simulations, a second-order polynomial curve is fitted to the strain energy-displacement data points. The bending stiffnesses determined by both methods are similar. The bending stiffnesses presented in the next section are calculated using Eq. (2).

### 2.3. Buckling

The buckling simulations are conducted similarly to the tensile simulations, with the difference being that the applied displacement is compressive rather than tensile and is applied to both ends of the nanobeam. The simulations correspond to the buckling problem of fixed-fixed nanobeams, as depicted in Fig. 4. The applied compressive strain rates for each case will be presented in the next section. The displacements of atoms in the upper and lower regions along the  $x$ - and  $y$ -axis are constrained. During the deformation, the temperature is kept constant and equal to 1 K using the NVT ensemble.

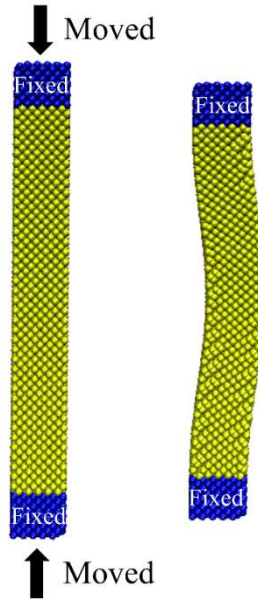


**Fig. 4** Undeformed and deformed silicon nanobeam after the compressive deformation.

The onset of buckling is identified by the point at which the strain energy-strain or force-strain curves experience a sudden drop. This depicted in Fig. 5 for a silicon nanobeam with  $L_z = 27.15$  nm,  $L_x = 3.258$

nm, and  $L_x = 2.715$  nm. The buckling load is the force exerted on the upper or lower regions when buckling begins.

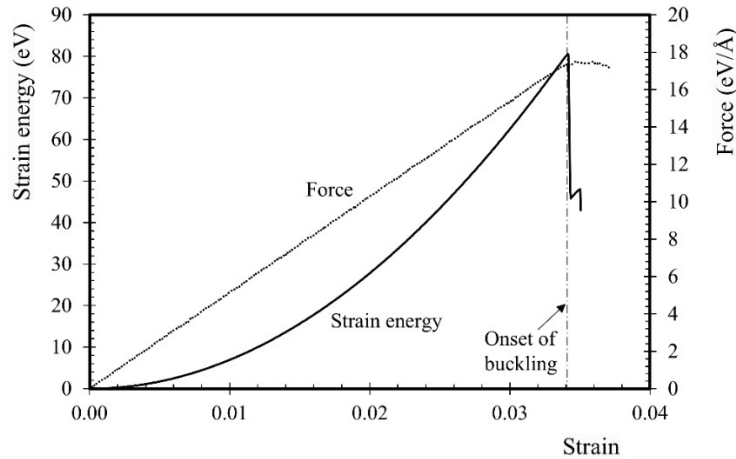


**Fig. 5** Strain energy-strain and force-strain curves during the compression of a silicon nanobeam with  $L_z = 27.15$  nm,  $L_x = 3.258$  nm, and  $L_y = 2.715$  nm.

## 2.4. Free Transverse Vibration

The fundamental natural frequencies of free transverse vibration in cantilever silicon nanobeams are investigated. For this analysis, the atoms within the simulation box are divided into fixed, mobile, and excitation regions, as illustrated in Fig. 6.

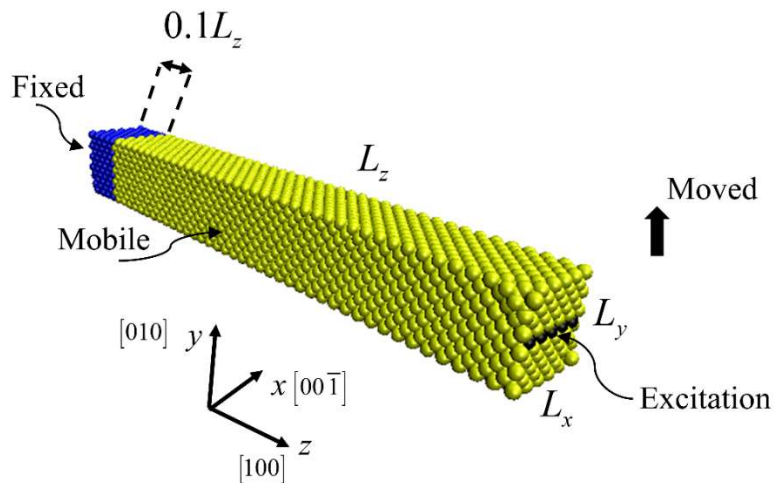


**Fig. 6** Configuration of the transverse vibration simulation.

All degrees of freedom of the atoms in the fixed region are constrained, replicating the boundary conditions of a cantilever beam. The atoms in the excitation region are located on the exterior cross-section at the middle of the thickness. To initiate the first mode of vibration within the linear elastic

regime, the atoms in the excitation region are displaced up to  $0.015L_z$  at a constant velocity along the  $y$ -axis, while their movement in other directions is restricted. Throughout the deformation process, the temperature is maintained at 1 K using the NVT ensemble. After this, all atoms, except those in the fixed region, are allowed to vibrate freely under the NVE ensemble.

During the free vibration of the nanobeam, the coordinates of the atoms along the  $y$ -axis within the excitation region are recorded over time  $t$ . Since the nanobeam is allowed to vibrate freely, a sinusoidal function of the form  $b_1 \sin(2\pi 10^{-3} \omega t + b_1)$  is fitted to the recorded coordinates, where  $\omega$  represents the vibration frequency of the cantilever beam in GHz. This procedure for the determination of the natural frequency of the silicon nanobeam with  $L_z = 21.72$  nm, and  $L_x = L_y = 2.715$  nm is illustrated in Fig. 7.

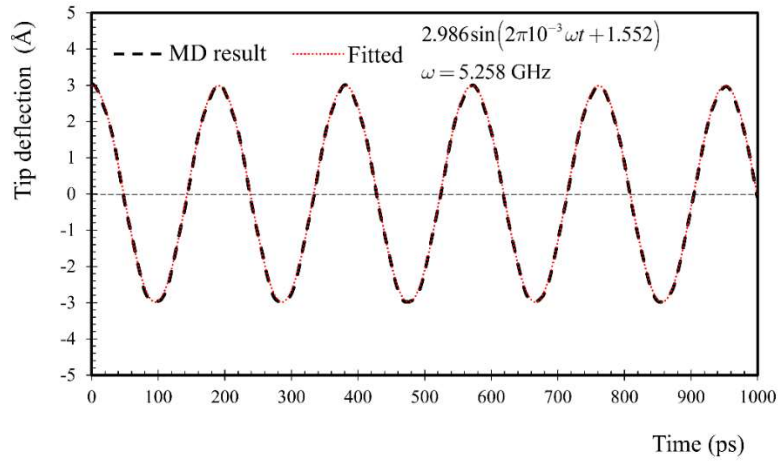


**Fig. 7** The amplitude of vibration predicted by the MD simulation and the corresponding fitted curve showing the frequency of 5.258 GHz. The results refer to the silicon beam with  $L_z = 21.72$  nm, and  $L_x = L_y = 2.715$  nm.

Time is measured relative to the onset of free vibration.

### 3. Results and Discussion

A comprehensive set of benchmark solutions is presented in this section for the size-dependent tension, bending, buckling, and free transverse vibration of silicon nanobeams. Three different types of size effects are investigated: (i) the scale effect, where the length, in-plane thickness, and out-of-plane width of the beams remain proportional; (ii) the thickness effect, where only the thickness varies while the other dimensions remain constant; and (iii) the length effect, where the length changes while the other dimensions are held constant. The size effect related to variations in the out-of-plane width is not studied. The data presented in this section can be used to verify size-dependent beam models based on

nonclassical continuum mechanics theories. Note that the specified dimensions given for the nanobeams refer to their dimensions before the initiation of the MD simulations, as these dimensions slightly change during the equilibrium phase of the simulations.

### 3.1. Scale Effect

This section analyzes beams with different aspect ratios to study the scale effect. The results for these slender and short beams provide essential data for verifying advanced models based on Euler-Bernoulli and Timoshenko beam theories.

#### 3.1.1 Tension

Silicon nanobeam with the dimensions of  $L_x = L_y = Sa_0$  and  $L_z = 15Sa_0$  where  $a_0$  is the lattice constant equal to  $5.43 \text{ \AA}$  are considered. Fig. 8 illustrates the variation of the Young modulus of the nanobeam along  $[100]$  crystallographic direction as the scale factor  $S$  varies from 2 to 20. The applied strain rate is equal to  $3.25 \times 10^6 \text{ s}^{-1}$ . The smallest and largest nanobeams have lengths of  $16.29 \text{ nm}$  and  $162.9 \text{ nm}$ , respectively. The simulations of these nanobeams involve  $1,489$  and  $1,182,001$  silicon atoms. It is evident from the figure that Young modulus decreases by more than 25% as the nanobeam size decreases. The largest silicon beam, with dimensions of  $162.9 \times 10.86 \times 10.86 \text{ nm}^3$ , exhibits a Young modulus of  $99.16 \text{ GPa}$ , which is very close to the value of  $100.16 \text{ GPa}$  reported in [46] for bulk silicon along the  $[100]$  crystallographic direction using MD simulations and the Stillinger-Weber potential.

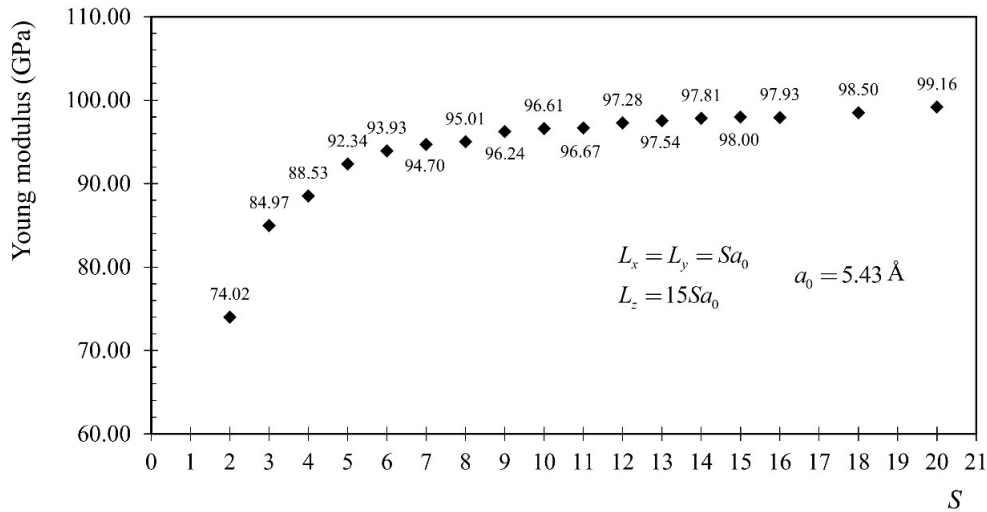


**Fig. 8** Young modulus of silicon nanobeams with  $L_x = L_y = Sa_0$  and  $L_z = 15Sa_0$  where  $a_0$  is the lattice constant equal to  $5.43 \text{ \AA}$  on varying the scale factor,  $S$ .

To investigate the effect of aspect ratio on the size-dependent Young's modulus, tensile simulations are performed on short silicon beams with the dimensions of  $L_x = L_y = Sa_0$  and  $L_z = 6Sa_0$ . The applied strain rate is equal to  $3.25 \times 10^6 \text{ s}^{-1}$ . The Young moduli of short beams with an aspect ratio of 6 are shown in Fig. 9. Comparing Fig. 8 and Fig. 9 shows that the aspect ratio slightly affects Young's modulus.

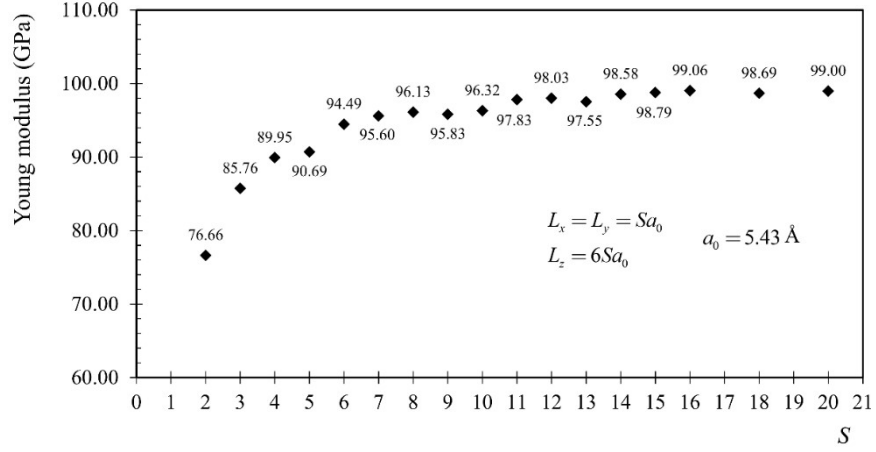


**Fig. 9** Young modulus of silicon nanobeams with  $L_x = L_y = Sa_0$  and  $L_z = 6Sa_0$  where  $a_0$  is the lattice constant equal to  $5.43 \text{ \AA}$  on varying the scale factor,  $S$ .

### 3.1.2 Bending

Silicon nanobeams with the cross-section of  $L_x = L_y = Sa_0$  and lengths of  $L_z = 15Sa_0$  and  $L_z = 6Sa_0$  where  $a_0$  is the lattice constant equal to  $5.43 \text{ \AA}$  are considered under bending. The applied deformation rates along the  $x$ -axis for the long and short beams are equal to  $534 \times 10^6$  and  $213.6 \times 10^6 \text{ \AA s}^{-1}$ , respectively. The bending stiffnesses obtained from the MD simulations are tabulated in Table 1.

**Table 1** The bending stiffnesses (N/m) obtained from the MD simulations of silicon nanobeams with the cross-section of  $L_x = L_y = Sa_0$ , where  $a_0$  is the lattice constant equal to  $5.43 \text{ \AA}$ . Results are presented for two different nanobeams with lengths of  $L_z = 15Sa_0$  and  $L_z = 6Sa_0$ . The applied deformation rates along the  $x$ -axis for the long and short beams are equal to  $534 \times 10^6$  and  $213.6 \times 10^6 \text{ \AA s}^{-1}$ , respectively.

$S$	$k_{L_z=15Sa_0}$ (N/m)	$k_{L_z=6Sa_0}$ (N/m)	$S$	$k_{L_z=15Sa_0}$ (N/m)	$k_{L_z=6Sa_0}$ (N/m)
2	0.016189	0.290744	11	0.166892	2.535021
3	0.035919	0.536150	12	0.190265	2.771907
4	0.052568	0.789245	13	0.210648	2.951399
5	0.071684	0.971311	14	0.225935	3.252475

6	0.088088	1.307966	15	0.232337	3.519845
7	0.108635	1.540450	16	0.245133	3.767374
8	0.114329	1.769943	18	0.288071	-
9	0.146385	1.943139	20	0.333253	-
10	0.149012	2.204328	-	-	-

To demonstrate the size effect on bending stiffness, the ratios between the MD results and those predicted by the classical beam model are illustrated in Fig. 10, with the scale factor  $S$  varying from 2 to 20. The closed-form solution for the bending stiffness of a fixed-guided beam on the  $x$ - $z$  plane, based on the classical beam model, is given by  $k_{\text{large}} = EL_y (L_x/L_z)^3$ . Here,  $E$  represents the Young modulus of a sufficiently large silicon beam along the  $z$ -axis, determined to be 99.16 GPa (see Fig. 8). The bending stiffnesses of the long and short silicon nanobeams based on the classical beam model are given by  $0.01595 \times S$  and  $0.24929 \times S$  N/m, respectively. Note that this closed-form solution neglects the contributions of shear deformations.

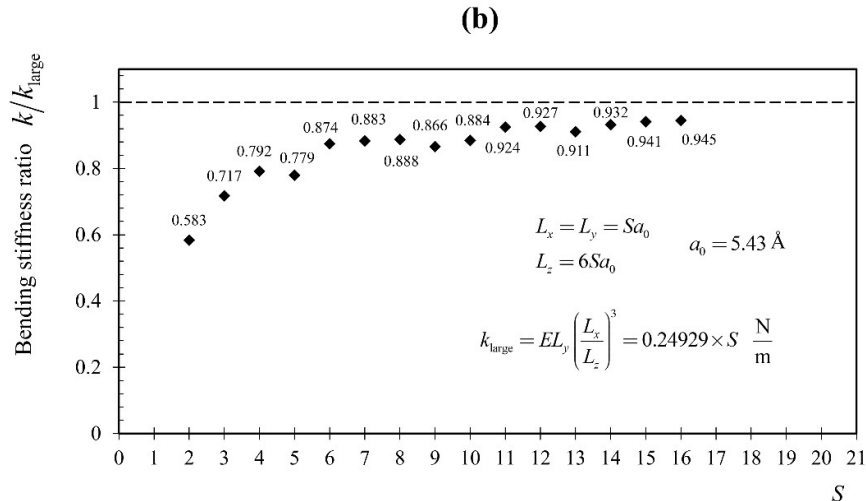
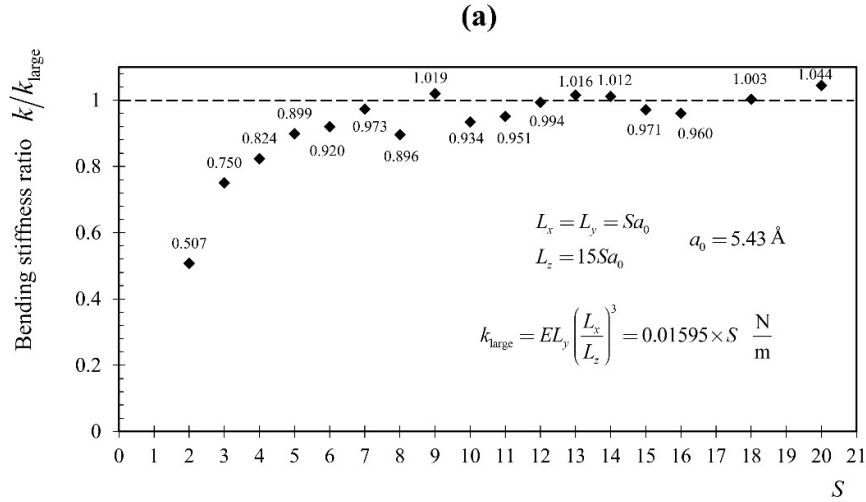


**Fig. 10** The ratios between the bending stiffnesses predicted by the MD simulations and those determined by the classical beam model on varying the scale factor,  $S$ , for the beams with aspect ratios (a) 15, and (b) 6.

The results presented in Fig. 10 illustrate that the bending stiffness of both long and short silicon nanobeams is size-dependent. In both cases, the MD results deviate more from the classical beam model as the scale factor decreases, consistent with the observations made for the tensile simulations. As the scale factor increases, the MD and classical beam model predictions for the long beam nearly coincide. However, for the short beam at high scale factor values, the results of the MD simulations slightly differ from those of the classical beam model due to the neglect of shear deformations. The results also confirm that the size effect in the bending stiffness depends on the aspect ratio of the nanobeam.

### 3.1.3 Buckling

Silicon nanobeams with the cross-section of  $L_x = L_y = Sa_0$  and lengths of  $L_z = 15Sa_0$  and  $L_z = 8Sa_0$  where  $a_0$  is the lattice constant equal to 5.43 Å are considered under buckling loading. The applied compressive strain rates along the  $z$ -axis for the long and short beams equal  $3.07 \times 10^6 \text{ s}^{-1}$  and  $9.21 \times 10^6 \text{ s}^{-1}$ , respectively. These strain rates are selected to ensure quasi-static loading conditions while maintaining affordable computational costs.

The buckling loads are normalized using Euler's formula and the results are shown in Fig. 11. The Euler's formula is given in the figure, where  $E$  represents the Young modulus of a sufficiently large silicon beam along the  $z$ -axis, determined to be 99.16 GPa (see Fig. 8). For both aspect ratios, smaller beams, i.e., those with lower scale factors, buckle at significantly lower forces than predicted by the classical model, due to the size effect. As the scale factor increases, the results of the MD simulations converge with those of Euler's formula. For beams with the higher aspect ratio, the predictions of both models nearly coincide for scale factors greater than 9. However, a gap remains between the MD simulations and Euler's formula for beams with the lower aspect ratio, even at larger scale factors, primarily because Euler's formula neglects the contribution of shear deformations in the buckling behavior of beams with low aspect ratios.

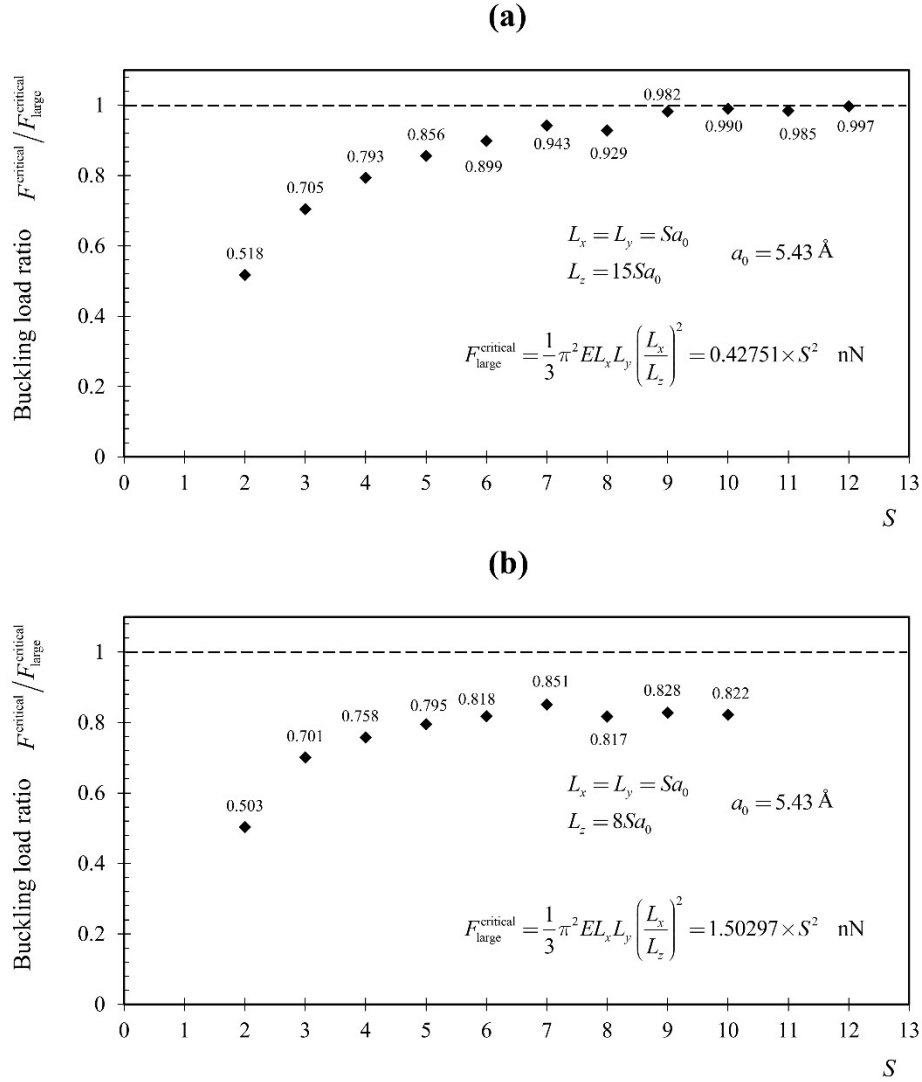


**Fig. 11** The ratios between the buckling loads predicted by the MD simulations and those determined by the classical beam model on varying the scale factor,  $S$ , for the beams with aspect ratios (a) 15, and (b) 8.

### 3.1.4 Free Transverse Vibration

Free transverse vibration simulations are performed on silicon nanobeams with the cross-section of  $L_x = L_y = Sa_0$  and lengths of  $L_z = 15Sa_0$  and  $L_z = 6Sa_0$  where  $a_0$  is the lattice constant equal to 5.43 Å. To highlight the size effect on beam frequency, the MD results are normalized against the closed-form solution based on the classical beam model, as shown in the figure. The Young's modulus and silicon density are 99.16 GPa and 2330 kg/m<sup>3</sup>, respectively. The results are presented in Fig. 12. The discrepancy between the frequencies predicted by the MD simulations and the classical beam model is greater for nanobeams with smaller scale factors, reflecting a stronger size effect.

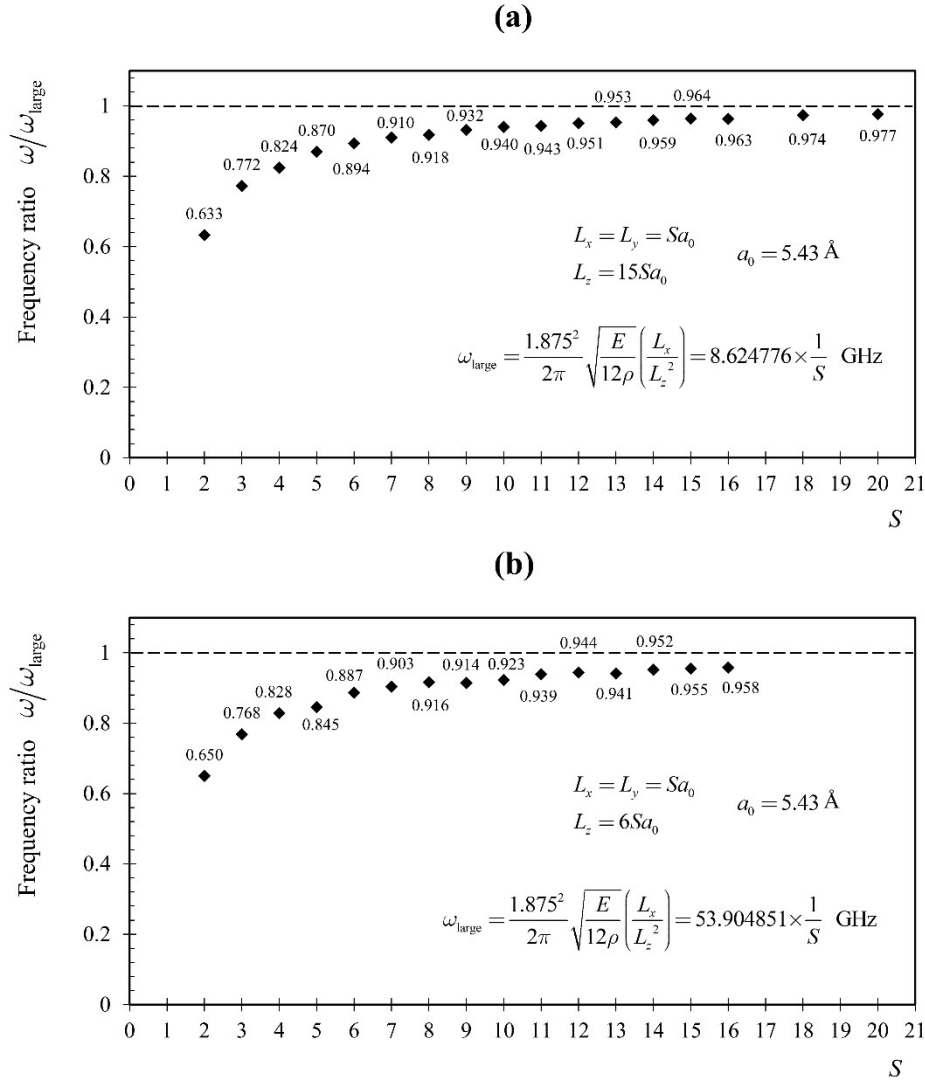


**Fig. 12** The ratios between the natural frequencies predicted by the MD simulations and those determined by the classical beam model on varying the scale factor,  $S$ , for the beams with aspect ratios (a) 15, and (b) 6.

A comparison of the figures presented in Section 3.1 reveals an important insight: the softening size effect in silicon nanobeams depends on both the aspect ratio of the beam and the type of problem, whether it involves bending, buckling, or vibration.

### 3.2. Thickness Effect

This section examines size effect resulting from variations in in-plane thickness. As in the previous section, simulations are conducted for the tension, bending, buckling, and transverse vibration of silicon nanobeams. The data presented here is especially important for verifying models that account for through-thickness size effects, such as those based on surface elasticity.

### 3.2.1 Tension

Silicon nanobeams with dimensions  $L_x = Xa_0$ ,  $L_y = 5a_0$  and  $L_z = 50a_0$  where  $a_0$  is the lattice constant equal to 5.43 Å, are considered. A set of tensile simulations is performed by varying the in-plane thickness parameter,  $X$ , while keeping the length and out-of-plane width of the nanobeams constant. The measured Young's modulus of the nanobeam along the [100] crystallographic direction is shown in Fig. 13, with  $X$  ranging from 2 to 10. In all simulations, the atoms in the upper region of the nanobeams, as shown in Fig. 1, are displaced upward at a constant velocity of  $10^9$  Å s<sup>-1</sup>. The figure clearly illustrates the size effect on the Young's modulus of the nanobeams.

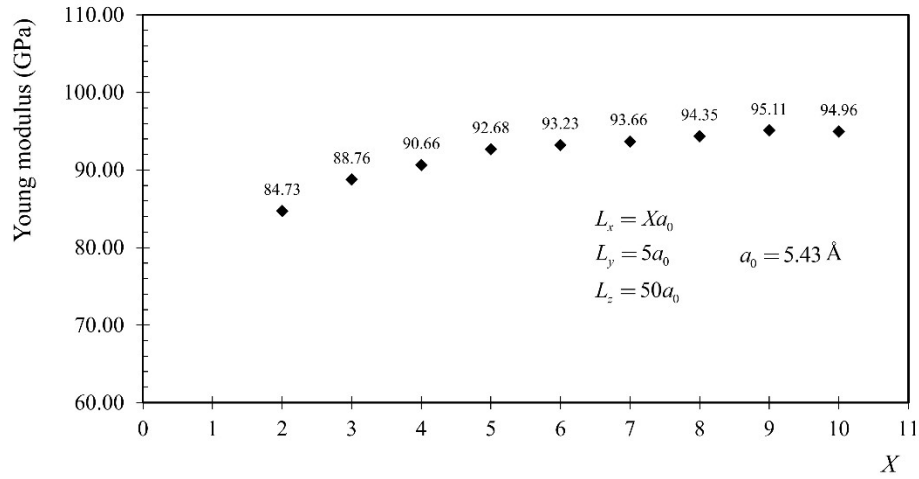


**Fig. 13** Young moduli of silicon nanobeams with  $L_x = Xa_0$ ,  $L_y = 5a_0$  and  $L_z = 50a_0$  where  $a_0$  is the lattice constant equal to 5.43 Å on varying the thickness parameter,  $X$ .

### 3.2.2 Bending

To illustrate the thickness-dependent size effect on bending stiffness, silicon nanobeams with dimensions  $L_x = Xa_0$ ,  $L_y = 5a_0$  and  $L_z = 50a_0$  where  $a_0$  is the lattice constant equal to 5.43 Å, are simulated. The applied deformation rate along the  $x$ -axis is  $10^9$  Å/s. The bending stiffness values obtained from the MD simulations,  $k_{\text{MD}}$ , along with the predictions from the classical model,  $k_{\text{classical}}$ , are shown in Fig. 14. The closed-form solution derived from the classical model, assuming Young's modulus of 99.16 GPa for silicon along the [100] crystallographic direction, is shown in the figure. As evident from the figure, the MD data deviate from the classical model predictions due to the size effect. Unlike the trend observed in the previous section for the scale effect, the ratios between the results of the MD simulations and classical

models,  $k_{\text{MD}}/k_{\text{classical}}$ , do not follow a consistent pattern. In the cases considered, this ratio ranges from 0.83 to 0.90.

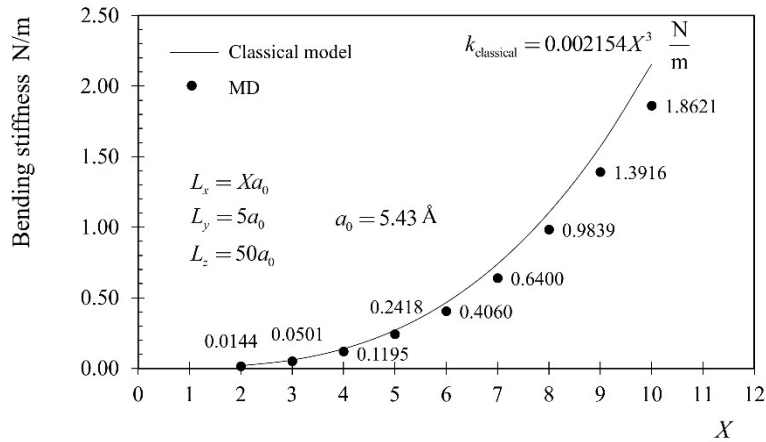


**Fig. 14** Bending stiffnesses of silicon nanobeams with  $L_x = Xa_0$ ,  $L_y = 5a_0$  and  $L_z = 50a_0$  where  $a_0$  is the lattice constant equal to 5.43 Å on varying  $X$ . Beams are deformed in the  $x$ - $z$  plane, so that  $L_x$  represents the in-plane thickness.

### 3.2.3 Buckling

Silicon nanobeams with dimensions  $L_x = Xa_0$ ,  $L_y = 10a_0$  and  $L_z = 50a_0$  where  $a_0$  is the lattice constant equal to 5.43 Å are considered under buckling loading. Simulations are conducted for the thickness parameter  $X$ , ranging from 2 to 8. In all cases, since  $L_x < L_y$ , the nanobeams buckle in the  $x$ - $z$  plane. Since the buckling strain increases significantly with increasing  $X$ , it is not feasible to use the same applied deformation rate for all simulations. To manage computational costs, the applied deformation rate is increased with  $X$  to ensure that the nanobeams buckle within 3.5 ns of simulation. For example, the buckling of the shortest nanobeam with  $X = 2$  is simulated by displacing the atoms in the upper and lower regions at a velocity of  $250 \times 10^6$  Å/s towards each other. For the nanobeam with  $X = 8$ , the velocity is 16.5 times higher.

The measured buckling loads, along with those predicted by Euler's formula, are shown in Fig. 15. Euler's formula, presented in the figure, assumes Young's modulus of 99.16 GPa. The figure illustrates the thickness-dependent size effect on the critical buckling loads, as the results from the two models diverge.

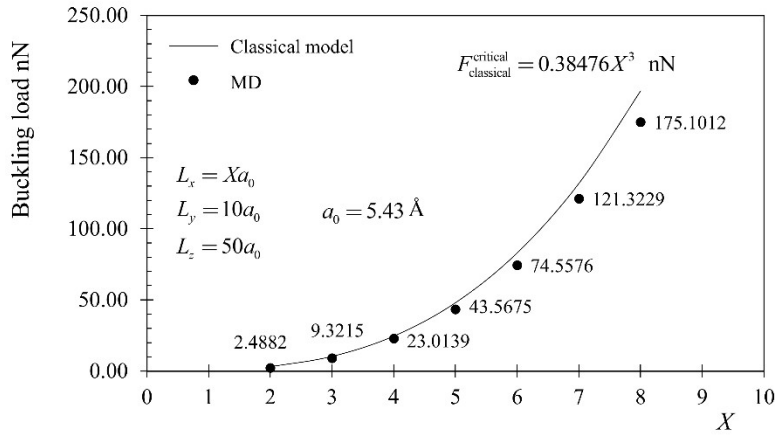


**Fig. 15** Buckling loads of silicon nanobeams with  $L_x = Xa_0$ ,  $L_y = 10a_0$  and  $L_z = 50a_0$  where  $a_0$  is the lattice constant equal to 5.43 Å on varying  $X$ . Beams buckle in the  $x$ - $z$  plane, so that  $L_x$  represents the in-plane thickness.

### 3.2.4 Free Transverse Vibration

Silicon nanobeams with dimensions  $L_x = 5a_0$ ,  $L_y = Xa_0$  and  $L_z = 50a_0$  where  $a_0$  is the lattice constant equal to 5.43 Å, are simulated to investigate the effect of thickness on natural frequencies. The frequencies predicted by MD simulations for nanobeams with thickness parameter  $X$ , ranging from 2 to 10, are shown in Fig. 16, alongside the predictions from the classical model. Both models predict a linear variation in frequency as the thickness parameter  $X$  changes; however, the results diverge due to the thickness size effect.

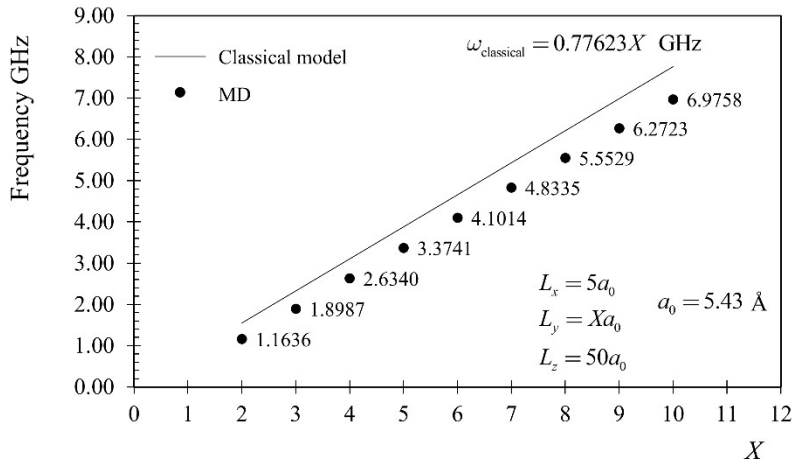


**Fig. 16** Natural frequencies of silicon nanobeams with  $L_x = 5a_0$ ,  $L_y = Xa_0$  and  $L_z = 50a_0$  where  $a_0$  is the lattice constant equal to 5.43 Å on varying  $X$ . Beams vibrate in the  $x$ - $z$  plane, so that  $L_x$  represents the thickness.

### 3.3. Length Effect

The size effect associated with variations in nanobeam length is examined in this section. Simulations are conducted for tension, bending, buckling, and transverse vibration of silicon nanobeams, with their lengths varied while the other dimensions remain constant.

#### 3.3.1 Tension

Results presented in Fig. 17 refer to the Young modulus of silicon nanobeams with  $L_x = 5a_0$ ,  $L_y = 5a_0$  and  $L_z = 20Xa_0$  where  $a_0$  is the lattice constant equal to 5.43 Å on varying the length parameter,  $X$ . The applied strain rate is equal to  $3.96 \times 10^6 \text{ s}^{-1}$ . It is evident that changing only the length of the nanobeam slightly reduces the Young modulus of silicon nanobeams.

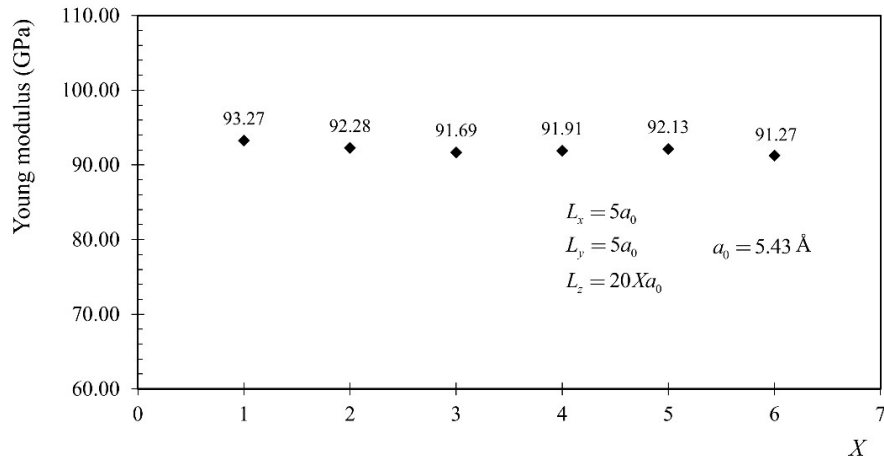


**Fig. 17** Young moduli of silicon nanobeams with  $L_x = 5a_0$ ,  $L_y = 5a_0$  and  $L_z = 20Xa_0$  where  $a_0$  is the lattice constant equal to 5.43 Å on varying the length parameter,  $X$ .

#### 3.3.2 Bending

The bending stiffness of silicon nanobeams with dimensions  $L_x = 5a_0$ ,  $L_y = 5a_0$  and  $L_z = 20Xa_0$  where  $a_0$  is the lattice constant equal to 5.43 Å, are presented in Fig. 18 by varying the length parameter,  $X$ , from 1 to 6. The applied deformation rate along the  $x$ -axis is  $X \times 430 \times 10^6 \text{ \AA/s}$ . Both the bending stiffnesses obtained from the MD simulations and the classical model are presented. For the classical model, a closed-form solution is derived, as shown in the figure, assuming Young's modulus of 99.16 GPa. Note that the vertical axis is presented on a logarithmic scale. The discrepancy between the results of the two models is attributed to the length-dependent size effect.

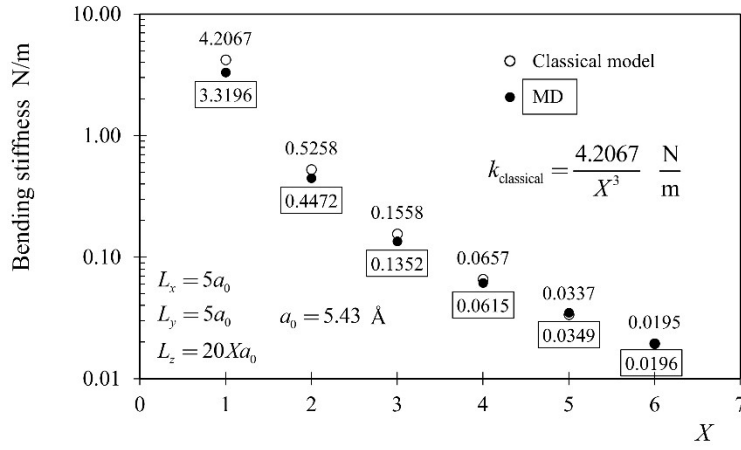


**Fig. 18** Bending stiffnesses of silicon nanobeams with  $L_x = 5a_0$ ,  $L_y = 5a_0$  and  $L_z = 20Xa_0$  where  $a_0$  is the lattice constant equal to 5.43 Å on varying the length parameter,  $X$ . Note that the vertical axis is presented on a logarithmic scale.

### 3.3.3 Buckling

For the buckling simulations, the same silicon nanobeams with dimensions  $L_x = 5a_0$ ,  $L_y = 5a_0$  and  $L_z = 20Xa_0$  where  $a_0$  is the lattice constant equal to 5.43 Å, are considered. The buckling loads determined by the MD simulations are shown in Fig. 19 for the length parameter  $X$ , ranging from 2 to 6. As the buckling strain decreases with increasing  $X$ , the applied deformation rate is reduced for longer nanobeams. For example, the buckling of the shortest nanobeam with  $X = 2$  is simulated by displacing the atoms in the upper and lower regions at a velocity of  $2 \times 10^9$  Å/s. For the longest nanobeam with  $X = 6$ , the velocity is reduced to  $240 \times 10^6$  Å/s. The buckling loads predicted by Euler's formula are also presented in Fig. 19, assuming Young's modulus of 99.16 GPa. The figure illustrates the length-dependent size effect on the critical buckling loads, with the results from the two models showing a clear deviation.

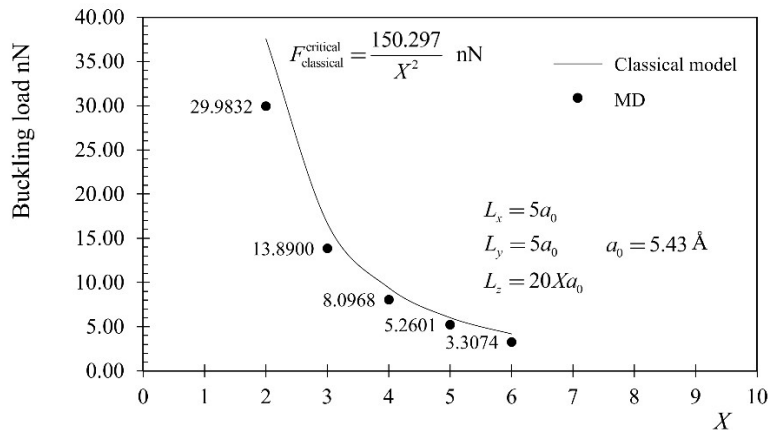


**Fig. 19** Buckling loads of silicon nanobeams with  $L_x = 5a_0$ ,  $L_y = 5a_0$  and  $L_z = 20Xa_0$  where  $a_0$  is the lattice constant equal to 5.43 Å on varying the length parameter,  $X$ .

### 3.3.4 Free Transverse Vibration

The MD simulations are applied to determine the natural frequencies of silicon nanobeams with dimensions  $L_x = 5a_0$ ,  $L_y = 5a_0$  and  $L_z = 20Xa_0$  where  $a_0$  is the lattice constant equal to 5.43 Å. Fig. 20 presents the results for nanobeams with the length parameter  $X$ , ranging from 1 to 6. The predictions from the classical model are also included to emphasize the length-dependent size effect on the natural frequencies.

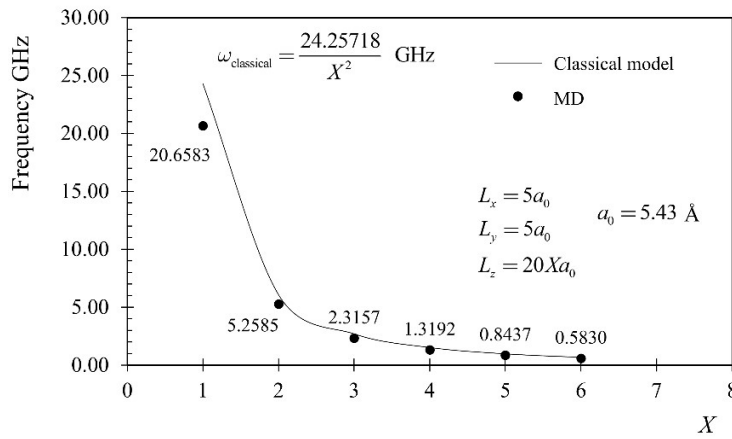


**Fig. 20** Natural frequencies of silicon nanobeams with  $L_x = 5a_0$ ,  $L_y = 5a_0$  and  $L_z = 20Xa_0$  where  $a_0$  is the lattice constant equal to 5.43 Å on varying the length parameter,  $X$ .

## 4. Conclusions

Size-dependent mechanical response of nanobeams has been intensively studied in the literature. This well-investigated research line resulted in the development of numerous nonclassical continuum mechanics-based beam theories. However, in many cases, the application of such theories in the design of the nanobeams in smart devices is hindered due to lack of a proper verification. In this paper, the classical MD method has been applied to generate comprehensive atomistic benchmark results for the tension, bending, buckling, and free transverse vibration of silicon nanobeams with square or rectangular cross-sections. Large-scale MD simulations, involving up to one million atoms allowed us to study three different kinds of size effects. First, the length, thickness, and width of the nanobeams are kept proportional and MD modeling is conducted while the scale of the beam changes. Second, nanobeams are modeled by changing only their length or thickness. The numerical values of the Young's moduli,

bending stiffnesses, buckling loads, and natural frequencies are presented confirming a softening size effect in the mechanical response of the silicon nanobeams with smaller dimensions. It has been confirmed that the type of the mechanical problem and the length-to-thickness ratios change the size effect intensity.

The comprehensive MD benchmark solutions presented in this work facilitate the verification and refinement of nonclassical continuum-based modeling approaches for miniaturized beams. Therefore, this study contributes to enhancing the design and performance of smart miniaturized devices that use micro- or nanobeams.

## **Funding**

The author gratefully acknowledges the financial support provided by the National Science Centre (NCN) in Poland through the grant agreement No: UMO-2022/47/D/ST8/01348. The author gratefully acknowledges Polish high-performance computing infrastructure PLGrid (HPC Centers: WCSS, ACK Cyfronet AGH) for providing computer facilities and support within computational grant no. PLG/2024/017086.

## **Declaration of interests**

The author declares that he has no known competing financial interests or personal relationships that could have appeared to influence the work reported in this paper.

## **References**

- [1] S.V. Kalinin, E. Karapetian, M. Kachanov, Nanoelectromechanics of piezoresponse force microscopy, *Phys. Rev. B* 70 (2004) 184101. <https://doi.org/10.1103/PhysRevB.70.184101>.
- [2] E. Karapetian, M. Kachanov, S.V. Kalinin, Nanoelectromechanics of piezoelectric indentation and applications to scanning probe microscopies of ferroelectric materials, *Philosophical Magazine* 85 (2005) 1017–1051. <https://doi.org/10.1080/14786430412331324680>.
- [3] B. Ilic, D. Czaplewski, M. Zalalutdinov, H.G. Craighead, P. Neuzil, C. Campagnolo, C. Batt, Single cell detection with micromechanical oscillators, *Journal of Vacuum Science & Technology B: Microelectronics and Nanometer Structures Processing, Measurement, and Phenomena* 19 (2001) 2825–2828. <https://doi.org/10.1116/1.1421572>.
- [4] Ö. Civalek, B. Uzun, M.Ö. Yaylı, On nonlinear stability analysis of saturated embedded porous nanobeams, *International Journal of Engineering Science* 190 (2023) 103898. <https://doi.org/10.1016/j.ijengsci.2023.103898>.
- [5] S. Wang, W. Ding, Z. Li, B. Xu, C. Zhai, W. Kang, W. Yang, Y. Li, A size-dependent quasi-3D model for bending and buckling of porous functionally graded curved nanobeam, *International Journal of Engineering Science* 193 (2023) 103962. <https://doi.org/10.1016/j.ijengsci.2023.103962>.

- [6] A. Farajpour, M.H. Ghayesh, H. Farokhi, A review on the mechanics of nanostructures, *International Journal of Engineering Science* 133 (2018) 231–263. <https://doi.org/10.1016/j.ijengsci.2018.09.006>.
- [7] M.H. Ghayesh, A. Farajpour, A review on the mechanics of functionally graded nanoscale and microscale structures, *International Journal of Engineering Science* 137 (2019) 8–36. <https://doi.org/10.1016/j.ijengsci.2018.12.001>.
- [8] S.A. Faghidian, K.K. Żur, J.N. Reddy, A mixed variational framework for higher-order unified gradient elasticity, *International Journal of Engineering Science* 170 (2022) 103603. <https://doi.org/10.1016/j.ijengsci.2021.103603>.
- [9] S.A. Faghidian, Higher-order nonlocal gradient elasticity: A consistent variational theory, *International Journal of Engineering Science* 154 (2020) 103337. <https://doi.org/10.1016/j.ijengsci.2020.103337>.
- [10] S.A. Faghidian, Integro-differential nonlocal theory of elasticity, *International Journal of Engineering Science* 129 (2018) 96–110. <https://doi.org/10.1016/j.ijengsci.2018.04.007>.
- [11] H. Altenbach, V.A. Eremeyev, On the shell theory on the nanoscale with surface stresses, *International Journal of Engineering Science* 49 (2011) 1294–1301. <https://doi.org/10.1016/j.ijengsci.2011.03.011>.
- [12] N. Challamel, C.M. Wang, The small length scale effect for a non-local cantilever beam: a paradox solved, *Nanotechnology* 19 (2008) 345703. <https://doi.org/10.1088/0957-4484/19/34/345703>.
- [13] N. Challamel, J. Lerbet, C. m. Wang, Z. Zhang, Analytical length scale calibration of nonlocal continuum from a microstructured buckling model, *ZAMM - Journal of Applied Mathematics and Mechanics / Zeitschrift Für Angewandte Mathematik Und Mechanik* 94 (2014) 402–413. <https://doi.org/10.1002/zamm.201200130>.
- [14] G. Romano, R. Barretta, Nonlocal elasticity in nanobeams: the stress-driven integral model, *International Journal of Engineering Science* 115 (2017) 14–27. <https://doi.org/10.1016/j.ijengsci.2017.03.002>.
- [15] R.D. Mindlin, H.F. Tiersten, Effects of couple-stresses in linear elasticity, *Arch. Rational Mech. Anal.* 11 (1962) 415–448. <https://doi.org/10.1007/BF00253946>.
- [16] R.D. Mindlin, Micro-structure in linear elasticity, *Arch. Rational Mech. Anal.* 16 (1964) 51–78. <https://doi.org/10.1007/BF00248490>.
- [17] A.C. Eringen, Linear Theory of Micropolar Elasticity, *Journal of Mathematics and Mechanics* 15 (1966) 909–923.
- [18] A.C. Eringen, D.G.B. Edelen, On nonlocal elasticity, *International Journal of Engineering Science* 10 (1972) 233–248. [https://doi.org/10.1016/0020-7225\(72\)90039-0](https://doi.org/10.1016/0020-7225(72)90039-0).
- [19] M.E. Gurtin, A. Ian Murdoch, A continuum theory of elastic material surfaces, *Arch. Rational Mech. Anal.* 57 (1975) 291–323. <https://doi.org/10.1007/BF00261375>.
- [20] A. Carpinteri, Fractal nature of material microstructure and size effects on apparent mechanical properties, *Mechanics of Materials* 18 (1994) 89–101. [https://doi.org/10.1016/0167-6636\(94\)00008-5](https://doi.org/10.1016/0167-6636(94)00008-5).

- [21] F. Yang, A.C.M. Chong, D.C.C. Lam, P. Tong, Couple stress based strain gradient theory for elasticity, *International Journal of Solids and Structures* 39 (2002) 2731–2743. [https://doi.org/10.1016/S0020-7683\(02\)00152-X](https://doi.org/10.1016/S0020-7683(02)00152-X).
- [22] D.C.C. Lam, F. Yang, A.C.M. Chong, J. Wang, P. Tong, Experiments and theory in strain gradient elasticity, *Journal of the Mechanics and Physics of Solids* 51 (2003) 1477–1508. [https://doi.org/10.1016/S0022-5096\(03\)00053-X](https://doi.org/10.1016/S0022-5096(03)00053-X).
- [23] C.W. Lim, G. Zhang, J.N. Reddy, A higher-order nonlocal elasticity and strain gradient theory and its applications in wave propagation, *Journal of the Mechanics and Physics of Solids* 78 (2015) 298–313. <https://doi.org/10.1016/j.jmps.2015.02.001>.
- [24] H.-T. Thai, T.P. Vo, T.-K. Nguyen, S.-E. Kim, A review of continuum mechanics models for size-dependent analysis of beams and plates, *Composite Structures* 177 (2017) 196–219. <https://doi.org/10.1016/j.compstruct.2017.06.040>.
- [25] S.A. Faghidian, K.K. Żur, E. Pan, Stationary variational principle of mixture unified gradient elasticity, *International Journal of Engineering Science* 182 (2023) 103786. <https://doi.org/10.1016/j.ijengsci.2022.103786>.
- [26] S.A. Faghidian, H. Darban, Non-standard interface conditions in flexure of mixture unified gradient Nanobeams, *International Journal of Engineering Science* 204 (2024) 104127. <https://doi.org/10.1016/j.ijengsci.2024.104127>.
- [27] H. Darban, R. Luciano, M. Basista, Calibration of the length scale parameter for the stress-driven nonlocal elasticity model from quasi-static and dynamic experiments, *Mechanics of Advanced Materials and Structures* 30 (2023) 3518–3524. <https://doi.org/10.1080/15376494.2022.2077488>.
- [28] C. Liebold, W.H. Müller, Comparison of gradient elasticity models for the bending of micromaterials, *Computational Materials Science* 116 (2016) 52–61. <https://doi.org/10.1016/j.commatsci.2015.10.031>.
- [29] W. Sumelka, T. Blaszczyk, C. Liebold, Fractional Euler–Bernoulli beams: Theory, numerical study and experimental validation, *European Journal of Mechanics - A/Solids* 54 (2015) 243–251. <https://doi.org/10.1016/j.euromechsol.2015.07.002>.
- [30] Z. Li, Y. He, J. Lei, S. Han, S. Guo, D. Liu, Experimental investigation on size-dependent higher-mode vibration of cantilever microbeams, *Microsyst Technol* 25 (2019) 3005–3015. <https://doi.org/10.1007/s00542-018-4244-0>.
- [31] Z. Li, Y. He, J. Lei, S. Guo, D. Liu, L. Wang, A standard experimental method for determining the material length scale based on modified couple stress theory, *International Journal of Mechanical Sciences* 141 (2018) 198–205. <https://doi.org/10.1016/j.ijmecsci.2018.03.035>.
- [32] J. Lei, Y. He, S. Guo, Z. Li, D. Liu, Size-dependent vibration of nickel cantilever microbeams: Experiment and gradient elasticity, *AIP Advances* 6 (2016) 105202. <https://doi.org/10.1063/1.4964660>.
- [33] Y. Xie, J. Lei, S. Guo, S. Han, J. Ruan, Y. He, Size-dependent vibration of multi-scale sandwich micro-beams: An experimental study and theoretical analysis, *Thin-Walled Structures* 175 (2022) 109115. <https://doi.org/10.1016/j.tws.2022.109115>.
- [34] S. Narendar, D. Roy Mahapatra, S. Gopalakrishnan, Prediction of nonlocal scaling parameter for armchair and zigzag single-walled carbon nanotubes based on molecular structural mechanics, nonlocal elasticity and wave propagation, *International Journal of Engineering Science* 49 (2011) 509–522. <https://doi.org/10.1016/j.ijengsci.2011.01.002>.

- [35] A. Ghafouri Pourkermani, B. Azizi, H. Nejat Pishkenari, Vibrational analysis of Ag, Cu and Ni nanobeams using a hybrid continuum-atomistic model, *International Journal of Mechanical Sciences* 165 (2020) 105208. <https://doi.org/10.1016/j.ijmecsci.2019.105208>.
- [36] H.N. Pishkenari, B. Afsharmanesh, F. Tajaddodianfar, Continuum models calibrated with atomistic simulations for the transverse vibrations of silicon nanowires, *International Journal of Engineering Science* 100 (2016) 8–24. <https://doi.org/10.1016/j.ijengsci.2015.11.005>.
- [37] Y. Zhang, C. Wang, T. V.B.C, Assessment of timoshenko beam models for vibrational behavior of single-walled carbon nanotubes using molecular dynamics, *Advances in Applied Mathematics and Mechanics* 1 (2009) 89–106.
- [38] S.H. Park, J.S. Kim, J.H. Park, J.S. Lee, Y.K. Choi, O.M. Kwon, Molecular dynamics study on size-dependent elastic properties of silicon nanocantilevers, *Thin Solid Films* 492 (2005) 285–289. <https://doi.org/10.1016/j.tsf.2005.06.056>.
- [39] M. Shariati, B. Azizi, M. Hosseini, M. Shishesaz, On the calibration of size parameters related to non-classical continuum theories using molecular dynamics simulations, *International Journal of Engineering Science* 168 (2021) 103544. <https://doi.org/10.1016/j.ijengsci.2021.103544>.
- [40] Y.Y. Zhang, C.M. Wang, W.H. Duan, Y. Xiang, Z. Zong, Assessment of continuum mechanics models in predicting buckling strains of single-walled carbon nanotubes, *Nanotechnology* 20 (2009) 395707. <https://doi.org/10.1088/0957-4484/20/39/395707>.
- [41] H. Darban, R. Luciano, A. Caporale, M. Basista, Modeling of buckling of nanobeams embedded in elastic medium by local-nonlocal stress-driven gradient elasticity theory, *Composite Structures* 297 (2022) 115907. <https://doi.org/10.1016/j.compstruct.2022.115907>.
- [42] S. Plimpton, Fast Parallel Algorithms for Short-Range Molecular Dynamics, *Journal of Computational Physics* 117 (1995) 1–19. <https://doi.org/10.1006/jcph.1995.1039>.
- [43] W. Humphrey, A. Dalke, K. Schulten, VMD: Visual molecular dynamics, *Journal of Molecular Graphics* 14 (1996) 33–38. [https://doi.org/10.1016/0263-7855\(96\)00018-5](https://doi.org/10.1016/0263-7855(96)00018-5).
- [44] K. Kang, W. Cai, Size and temperature effects on the fracture mechanisms of silicon nanowires: Molecular dynamics simulations, *International Journal of Plasticity* 26 (2010) 1387–1401. <https://doi.org/10.1016/j.ijplas.2010.02.001>.
- [45] K. Mohammadi, A. Ali Madadi, Z. Bajalan, H. Nejat Pishkenari, Analysis of mechanical and thermal properties of carbon and silicon nanomaterials using a coarse-grained molecular dynamics method, *International Journal of Mechanical Sciences* 187 (2020) 106112. <https://doi.org/10.1016/j.ijmecsci.2020.106112>.
- [46] H.N. Pishkenari, B. Afsharmanesh, E. Akbari, Surface elasticity and size effect on the vibrational behavior of silicon nanoresonators, *Current Applied Physics* 15 (2015) 1389–1396. <https://doi.org/10.1016/j.cap.2015.08.002>.